Article:
Lishchuk, SV and Ettelaie, R (2016) Detachment force of particles with pinning of contact line from fluid bubbles/droplets. Langmuir, 32 (49). pp. 13040-13045. ISSN: 0743-7463

https://doi.org/10.1021/acs.langmuir.6b03546

Detachment force of particles with pinning of contact line from fluid bubbles/droplets

Sergey V. Lishchuk*,† and Rammile Ettelaie‡

Materials and Engineering Research Institute, Sheffield Hallam University, Howard Street, S1 1WB, UK, and Food Colloids Group, School of Food Science and Nutrition, University of Leeds, Leeds LS2 9JT, UK

E-mail: sergey.lishchuk@gmail.com

Abstract

Deformation of a spherical droplet or bubble, containing a pair of particles on its surface is considered when equal but opposite forces are applied to the particles. The particles are placed opposite each other thus providing a symmetrical problem which is more amenable to analytical treatment. We extend our previous calculations, concerning such arrangements with constant contact angles, to situations where now it is the contact line that is pinned on the surface of the particles. The force–displacement curves are calculated as the particles are pulled apart and was found to be linear for small displacements. However, it is also found that the "Hookean constant" for the pinned contact line problem is different to one derived for systems with a constant contact angle, being larger if the pinned line is at the equator of the particles.

*To whom correspondence should be addressed
†Materials and Engineering Research Institute, Sheffield Hallam University, Howard Street, S1 1WB, UK
‡Food Colloids Group, School of Food Science and Nutrition, University of Leeds, Leeds LS2 9JT, UK

Introduction

It is a common observation during the processes of spreading and wetting of solid surfaces by a liquid, that the advancing and receding contact angles are different to each other and often also to the equilibrium value of the contact angle.[1] In the extreme cases, the three phase contact line can become pinned due to the presence of imperfection, defects and inhomogeneities on the surface.[1–3] In such cases the contact angle is no longer uniquely defined but instead can take on a range of values determined by the external conditions to which the liquid is subjected (e. g. external forces). The phenomenon of pinning has significant implications for the behaviour of small particles at fluid–fluid interfaces and therefore in such processes as stability of particle-laden fluid interfaces in Pickering emulsions and bubbles,[4,5] in degassing of liquids using particle anti-foaming agents[6] and in separation of mineral particles by froth flotation technique.[7]

In our previous work[8] we calculated the deformation of a spherical droplet, resulting from the application of a pair of opposite forces applied to two particles located diametrically opposite each other at the two ends of the droplet. The free-energy analysis was used to calculate the force–distance curves for the generated restoring forces, arising from the displacement of the particles relative to each other.

In these previous calculations it was explicitly assumed that the contact line is free to slide along the surface of the particles. As mentioned, it is often the case that the contact line is pinned. In experimental studies pinning can be deliberately introduced by modifying the geometry of the surface.[9–11] Pinning is responsible for the hysteresis of the contact angle[1–3] and an unexpectedly slow relaxation of the position of the particles adsorbed at fluid interfaces towards equilibrium.[12,13] It also causes the modification of the detachment force of particles from fluid interfaces.[9–11] Recent AFM measurments with the three-phase contact line pinned at the probe allowed determination of the size-dependent stiffness of nanodroplets.[14]

The aim of this work is to extend the results of our previous study[8] to account for the

practically important and more relevant situations involving contact line pinning.

Model

In order to simplify the analysis, we consider a problem in which a droplet (or bubble) of radius R (in its undeformed state) has two particles of radius a adsorbed at its surface, placed diametrically opposite each other. This problem is equivalent to the description of the common experimental setups in which a particle is adsorbed on the hemispherical droplet which, in turn, is located on a flat substrate and forms free contact line with that substrate. The geometry of the system is shown in Figure 1a and follows from the one we used in our previously reported work.[8] The axially symmetric shape of the droplet is described by the function $z(\rho)$, in the cylindrical coordinate system.

The symmetry of the problem and hence the mathematical formulation is identical to one of the earlier papers on an axisymmetric capillary bridge by Orr, Scriven and Rivas.[15] We apply equal but opposite forces to each particle as is shown schematically in Figure 1a. The symmetrical nature of the problem, considered in this way, provides significant simplifications allowing us to obtain exact analytical expressions for the distortion of the shape of the spherical bubble, and hence the force vs displacement curves as the particles are pulled away from each other.

Displacement–force dependence

In this section we derive the explicit expression for the dependence of the external force F applied to the particles resulting in a displacement Δr from their equilibrium positions. As in our previous work,[8] the magnitude of the external force can be represented as a derivative of the free energy of the system, $\mathcal{F}$, with respect to distance $2r$ between the particles:

$$F = \frac{d\mathcal{F}}{d(2r)}. \tag{1}$$

Note that this is the external force applied to the particles and as such has the opposite sign to the force commonly represented in experimental plots,[10] where often the capillary forces pulling the particles back towards their equilibrium positions is reported. It can be viewed as the adhesive force, with which the particles "adhere" to the droplet.

Since the contact radius ρ_c (Figure 1b), in contrast with our previous work, is fixed here according to the assumption of contact line pinning, the only variable contribution to the free energy is determined by the surface tension γ of the interface between two fluids which can be written as

$$\mathcal{F} = \gamma S, \tag{2}$$

where S is the area of the fluid interface. The equilibrium shape of the interface can be obtained by minimizing the free energy (2) under the constraint of constant volume of the droplet. Gaseous bubbles can also be considered as incompressible if the particle-to-bubble size ratio is small and thus the distortion caused in the initial pressure of the bubble during particle displacement, is sufficiently small.[8]

The minimization of the free energy of the system under the constraint of constant volume of the droplet leads to the following results.[8] The shape of the droplet is unduloid[15,16] described by formula

$$z(\rho) = \rho_+ E(\varphi, k) + \frac{c\rho_0^2}{2\rho_+} F(\varphi, k) \tag{3}$$

where

$$\rho_+ = \sqrt{\frac{1 - c + \sqrt{1 - 2c}}{2}}\rho_0 \tag{4}$$

and

$$\rho_- = \sqrt{\frac{1 - c - \sqrt{1 - 2c}}{2}}\rho_0, \tag{5}$$

with ρ_0 and c constants that are determined by the volume of the droplet and the positions of the particles. Functions $F(\varphi, k)$ and $E(\varphi, k)$ are incomplete elliptic integrals of first and

second kind, respectively, where

$$\sin\varphi = \sqrt{\frac{\rho_+^2 - \rho^2}{\rho_+^2 - \rho_-^2}}, \tag{6}$$

and

$$k = \sqrt{1 - \frac{\rho_-^2}{\rho_+^2}}. \tag{7}$$

The cylindrical coordinates ρ and z are defined in Figure 1(a). The distance r of the center of each particle from the center of the droplet can be expressed in terms of the function $z(\rho)$ such that

$$r = z(\rho_c) - \sqrt{a^2 - \rho_c^2} \tag{8}$$

with displacement of the particle given by

$$\Delta r = r - R. \tag{9}$$

The free energy of the system, up to a constant term, was found to be[8]

$$\mathcal{F} = 4\pi\gamma\rho_+\rho_0 E(\varphi_c, k), \tag{10}$$

where

$$\sin\varphi_c = \sqrt{\frac{\rho_+^2 - \rho_c^2}{\rho_+^2 - \rho_-^2}}. \tag{11}$$

and γ denotes the surface tension. The volume of the distorted droplet can be integrated

and is found to be given by formula[8]

$$V = \frac{4\pi}{3}\left\{\left[\left(1-\frac{c}{4}\right)\rho_0^2 - \frac{3}{2}\rho_c^2\right]\rho_+ E(\varphi_c,k) - \left[\frac{\rho_-^2\rho_+}{2} + \frac{3}{4}\frac{c\rho_0^2\rho_c^2}{\rho_+}\right]F(\varphi_c,k) + \frac{\rho_c}{2}\sqrt{(\rho_+^2-\rho_c^2)(\rho_c^2-\rho_-^2)} + \frac{3}{2}\rho_c^2 r - \left[a^3 - (a^2-\rho_c^2)^{3/2}\right]\right\}. \tag{12}$$

Note that in deriving Eq. (12) one has to account for the regions occupied by the particles residing within the droplet. In the case $\alpha_c > \pi/2$ the volume of two spherical rings with sphere radius a and cylindrical hole radius ρ_c is equal to

$$\frac{4\pi}{3}\left(a^2-\rho_c^2\right)^{3/2}. \tag{13}$$

This corresponds to the volume at $\rho > \rho_c$ which lies inside the particles and hence is not part of the liquid. Therefore this volume should be subtracted from the total one, Eq. (12), to yield the actual volume of the fluid droplet. As the forces are incurred and the shape of the droplet alters, this volume nonetheless has to remain constant.

Further analysis is simplified if the particle-to-droplet size ratio,

$$\nu = \frac{a}{R}, \tag{14}$$

is small, $\nu \to 0$. In this case we can use the series expansions of the elliptic integrals at $\phi_c \to \pi/2$ and $k \to 1$[8]

$$F(\varphi_c,k) = -\ln\frac{(\kappa+\xi)\nu}{4} + o\left(\nu^0\right) \tag{15}$$

and

$$E(\varphi_c, k) = 1 - \left\{ \frac{\kappa^2}{2} + \frac{\mu^2}{16} \left[2 \ln \frac{(\kappa + \xi)\nu}{4} - \frac{\kappa - \xi}{\kappa + \xi} \right] \right\} \nu^2 + o\left(\nu^2\right), \tag{16}$$

where we have defined

$$\xi = \sqrt{\kappa^2 - \frac{\mu^2}{4}}, \tag{17}$$

$$\mu = \frac{c}{\nu} \tag{18}$$

and

$$\kappa = \frac{\rho_c}{a}. \tag{19}$$

With the constraint requiring the volume of the droplet to remain constant and using the above expansions, we can obtain the required expressions for the particle displacement, in the limit of small particles to droplet size ratio

$$\frac{\Delta r}{a} = -\frac{\mu}{4} \left[1 + 2 \ln \frac{(\kappa + \xi)\nu}{4} \right]. \tag{20}$$

The corresponding free energy of the system is then given by

$$\mathcal{F}(\mu) = -2\pi a^2 \gamma \left\{ \kappa^2 + \frac{\mu^2}{4} \left[\frac{\xi}{\kappa + \xi} + \ln \frac{(\kappa + \xi)\nu}{4} \right] \right\}. \tag{21}$$

These formulas express parametrically the free energy dependence of the system as a function of the displacement of the particles. The parameter μ characterizes the deformation of the droplet from its original spherical shape. Furthermore, we can also express the force as a function of μ by considering the derivative of the free energy with respect to displacement:

$$F(\mu) = \frac{1}{2} \frac{(\partial \mathcal{F}/\partial \mu)}{(\partial r/\partial \mu)}. \tag{22}$$

In its explicit form this equals

$$F = \pi a \gamma \mu. \tag{23}$$

Expressing the parameter μ from the above formula in terms of the applied force F and substituting this in the equation for the displacement of the particle, we can write explicitly the formula for the displacement–force relation as

$$\Delta r = -\frac{F}{4\pi\gamma}\left\{1 + 2\ln\left[\frac{\rho_c}{4R}\left(1 \pm \sqrt{1 - \left(\frac{F}{2\pi\gamma\rho_c}\right)^2}\right)\right]\right\}. \tag{24}$$

Here the two signs, $\pm$, correspond to the displacements of the particle before and after reaching the point of maximum force, respectively. The Hookean ("spring") constant defined as the ratio of force to displacement for small deviations of particle position from its equilibrium value is

$$k_{\mathrm{H}} \equiv \left(\frac{dF}{d\Delta r}\right)_{\Delta r \to 0} = \frac{4\pi\gamma}{2\ln\left(\frac{2R}{\rho_c}\right) - 1}. \tag{25}$$

In figure 2 we compare the displacement–force behavior for the cases of pinned contact line (Eq. 24) and our previous result for a system with a fixed contact angle of $\pi/2$, which is given by formula[8]

$$\frac{\Delta r}{a} = \sqrt{\frac{1 \mp \Phi}{2}} - \frac{F}{2\pi\gamma a}\left\{\frac{1}{2} + \ln\left[\frac{a}{8R}\left(1 \pm \Phi + \sqrt{2(1 \pm \Phi)}\right)\right]\right\}, \tag{26}$$

with

$$\Phi = \sqrt{1 - \left(\frac{F}{\pi\gamma a}\right)^2}. \tag{27}$$

Maximum displacement, detachment force and Hookean constant are all higher in the case of pinned contact line compared to the case of free contact line. It is straightforward to show using Eq. (24) that Hookean constant in the case of pinned constant line with the contact radius ρ_c equals Hookean constant for the case of free contact line[8] for larger particles of radius $a = e\rho_c$, where $e = 2.718\ldots$ is Euler's number.

Detachment of particles

As the external force acting on the particle is made larger, the displacement of the particle from its equilibrium position increases. The contact line remains pinned at the same position until a critical value for the particle displacement is reached. Subsequently, two scenarios are possible. First, the particle can detach from the fluid droplet by the rupture of the fluid bridge because beyond this critical point there is no stable state of the system with the pinned contact line. The second scenario involves the transition to free sliding of the contact line along the particle surface.

In order to establish the criterion which distinguishes these two mechanisms we write the explicit solution for the displacement–force dependence obtained for the case of the freely sliding contact line. In the limit of small particle to droplet size ratios the analytical expression for dependence between the force and the displacement of the particles is given parametrically by Eq. (23), where now[8]

$$\Delta r(\kappa_f) = a\left\{\sqrt{1-\kappa_f^2} - \frac{\mu}{4}\left[1 + 2\ln\frac{(\kappa_f+\xi)a}{4R}\right]\right\} \tag{28}$$

instead of Eq. (20) for pinned case, and

$$\mu = 2\kappa_f\left(\sqrt{1-\kappa_f^2}\sin\theta_f - \kappa_f\cos\theta_f\right). \tag{29}$$

Here the angle θ_f denotes the equilibrium contact angle between the fluid interface and the flat surface which, in the case of freely sliding contact line, is determined by surface tensions through Young's equation. The dimensionless parameter κ_f is related to the contact radius ρ_f, for the freely sliding contact line, and is given by

$$\kappa_f = \frac{\rho_f}{a}. \tag{30}$$

In Eqs (28) and (23) (in which μ is now a function of κ_f given by Eq. (29)), κ_f changes

between $\kappa_{\min}$ and 1, as ρ_f alters with displacement of the particle. The minimum value of κ_f, $\kappa_{\min}$, is determined by the solution of transcendental equation

$$\left(\frac{d\Delta r(\kappa_f)}{d\kappa_f}\right)_{\kappa_f=\kappa_{\min}} = 0. \tag{31}$$

If the transition to sliding contact line is possible, it occurs at the displacement of the particle at which the contact radius ρ_c of the pinned contact line equals contact radius ρ_f corresponding to the freely sliding case. The corresponding displacement is thus given by Eq. (28) where $\kappa_f = \kappa$. The applied force at this point, if required, can be obtained by inverting Eq. (24). Behavior of the system beyond this displacement is then described by the model relevant to the free contact line.[8] Note that the force abruptly decreases with the transition to the sliding regime, so in principle detachment can still occur at the same displacement. This regime is similar to the one described by Akbari and Hill,[17] who studied experimentally and theoretically the stability and breakup of liquid bridges with a free contact line on surfaces with contact-angle hysteresis. Akbari and Hill have identified the regime in which the stability of liquid bridges is lost during a transition from pinned to free interface.

In the case when $\kappa < \kappa_{\min}$, where $\kappa_{\min}$ is the solution of Eq. (31), there is no longer a stable solution for the sliding contact line case, and the detachment of the particle occurs without intermediate transition to a stable sliding regime. The maximum force,

$$F^* = 2\pi\gamma\rho_c, \tag{32}$$

is then attained at a particle position given by

$$\Delta r^* = \left[\ln\left(\frac{4R}{\rho_c}\right) - \frac{1}{2}\right]\rho_c \tag{33}$$

obtained from Eq. (24). The corresponding value of the contact angle θ at the same point

is found to be

$$\theta = \alpha_c - \left[\arctan z'(\rho)\right]_{\rho=\rho_c}, \tag{34}$$

where $z(\rho)$ is given by Eq. (3) and has its derivative (with respect to ρ) as follows

$$z'(\rho) = -\frac{\frac{1}{2}c\rho_0^2 + \rho^2}{\sqrt{\rho_0^2\rho^2 + \left(\frac{1}{2}c\rho_0^2 + \rho^2\right)^2}}. \tag{35}$$

Substituting Eq. (35) in Eq. (34) and taking the small-particle limit we obtain the following final expression for this contact angle, θ_c:

$$\theta_c = \alpha_c + \tan^{-1}\left(\frac{1}{\sqrt{2}}\right). \tag{36}$$

Comparison with experiment

In this section we compare our results with the experimental data by Ally et al.[10] In order to study the effect of sharp edges on adhesion of solid particle to air–liquid interfaces, Ally et al. modified spherical colloidal probes with a circumferential cut produced by focused ion beam milling technique. The interaction of the modified particles with water drops and bubbles was studied using the colloidal probe technique. When the modified particles were brought into contact with air–liquid interfaces and subsequently pulled away, the contact line remained pinned at the edge of the cut. Contact hysteresis between the approach and retraction components of the measured force curves was eliminated. The contact angle at the edge then takes on a range of values within the limits imposed by the Gibbs' criterion.[18] These limits determine the adhesion force. As such, the adhesion force is a function of the particle wettability but also edge geometry.

Figures 3 and 4 compare our theoretical calculations with the experimental data by Ally et al.[10] on the particle being detached for the surface of the air bubble and water droplet, respectively. The values of the contact angle at detachment, 82° and 76°, calculated using

Eq. (36), are less than the corresponding values 110° and 103° calculated by Ally et al.[10] from the average values of the adhesion force. The agreement in the displacement–force dependence is good for the case of the bubble (figure 3). In the case of the droplet (figure 4) the agreement is worse and the deviation from the theoretical result has the opposite sign to that for bubble. Moreover, maximum force is smaller and is observed at lower displacement than predicted by the theory here.

Different sources of the error are possible. The possible errors for the measurements are[19] (i) determination of the spring constant of the order of 10%, and (ii) the calibration of the scanning electron microscope and the determination of the contact line radius $\sim 5\%$.

Other sources of discrepancy may lie in applicability conditions for equation (24). This equation is valid if (i) the particle-to droplet size ratio, given by equation (14), is small so that truncation of the expansions (16) and (15) is justified, and (ii) Bond number, given by

$$\mathrm{Bo} = \frac{(\rho_w - \rho_a) g L^2}{\gamma}, \tag{37}$$

where ρ_w and ρ_a are densities of water and air, respectively, and g has the usual value $9.81\,\mathrm{m/s^2}$, is small enough so that gravity effects can be neglected. Equation (14), is well satisfied for $0.3\,\mu$L droplets/bubbles with the adsorbed particles having a size $\sim 2\,\mu$m, as used in the experiment.[10] However, substituting the diameter of the droplet,

$$D = \sqrt[3]{\frac{12V}{\pi}} \tag{38}$$

as the characteristic length L, we obtain $\mathrm{Bo} = 0.15$, which may not be sufficiently small to allow for neglect of gravity effects.

Conclusion

We have considered two identical spherical solid particles with sharp edges itched on them, adsorbed on the surface of, and located at the opposite poles of an incompressible fluid droplet. The free-energy analysis was used to calculate the force–distance curves for the generated restoring forces, arising from the displacement of the particles relative to each other.

The agreement of our results with the experimental data by Ally et al.[10] is good in the case of air bubble in water, but less so in the case of water droplet in air. We attribute the discrepancy to the effect of gravity which can be expected to give corrections of opposite signs depending on whether the system involves an air bubble in water or a water droplet in air. An account of gravity can be introduced in the theory as the extension of the present work.

Some other possible future extensions may involve different particle locations on a sessile droplet,[20] influence of contact line pinning on the capillary interaction between particles on a sessile droplet[21] and in assessing the stability of Pickering emulsions under the application of external fields. Finally, the influence of fluid dynamics under fast stretching conditions and time dependence variation of force as a result[22] could be of particular interest in future studies.

Acknowledgement

The authors thank Prof. Hans-Jürgen Butt and Dr Michael Kappl for providing their experimental data and useful discussions of the results.

References

(1) de Gennes, P. G. Wetting: statics and dynamics. *Rev. Mod. Phys.* **1985**, *57*, 827–863.

(2) Joanny, J. F.; Robbins, M. O. Motion of a contact line on a heterogeneous surface. *J. Chem. Phys.* **1990**, *92*, 3206–3212.

(3) Pitois, O.; Chateau, X. Small Particle at a Fluid Interface: Effect of Contact Angle Hysteresis on Force and Work of Detachment. *Langmuir* **2002**, *18*, 9751–9756.

(4) Binks, B. P. Particles as surfactants—similarities and differences. *Curr. Opin. Coll. Int. Sci.* **2002**, *7*, 21–41.

(5) Murray, B. S.; Ettelaie, R. Foam stability: proteins and nanoparticles. *Curr. Opin. Coll. Int. Sci.* **2004**, *9*, 314–320.

(6) Dickinson, E. *An Introduction to Food Colloids*; Oxford University Press, 1992.

(7) Ata, S. Phenomena in the froth phase of flotation — A review. *Int. J. Mineral Processing* **2012**, *102-103*, 1–12.

(8) Ettelaie, R.; Lishchuk, S. V. Detachment force of particles from fluid droplets. *Soft Matter* **2015**, *11*, 4251–4265.

(9) O'Brien, S. B. G. The Meniscus near a Small Sphere and Its Relationship to Line Pinning of Contact Lines. *J. Coll. Int. Sci.* **1996**, *183*, 51–56.

(10) Ally, J.; Kappl, M.; Butt, H.-J. Adhesion of particles with sharp edges to air–liquid interfaces. *Langmuir* **2012**, *28*, 11042–11047.

(11) Feng, D.-X.; Nguyen, A. V. How does the Gibbs inequality condition affect the stability and detachment of floating spheres from the free surface of water? *Langmuir* **2016**, *32*, 1988–1995.

(12) Kaz, D. M.; McGorty, R.; Mani, M.; Brenner, M. P.; Manoharan, V. N. Physical aging of the contact line on colloidal particles at liquid interfaces. *Nature Materials* **2012**, *11*, 138–142.

(13) Rahmani, A. M.; Wang, A.; Manoharan, V. N.; Colosqui, C. E. Colloidal particle adsorption at liquid interfaces: Capillary driven dynamics and thermally activated kinetics. *Soft Matter* **2016**, *12*, 6365–6372.

(14) Wang, S.; Wang, X.; Zhao, B.; Wang, L.; Qiu, J.; Zhou, L.; Dong, Y.; Li, B.; Lü, J.; Wang, Y.; Zhang, Y.; Zhang, L.; Hu, J. Size-Dependent Stiffness of Nanodroplets: A Quantitative Analysis of the Interaction between an AFM Probe and Nanodroplets. *Langmuir* **2016**, *32*, 11230–11235.

(15) Orr, F. M.; Scriven, L. E.; Rivas, A. P. Pendular rings between solids: meniscus properties and capillary force. *J. Fluid. Mech.* **1975**, *67*, 723–742.

(16) Hadzhilazova, M.; Mladenov, I. M.; Oprea, J. Unduloids and their geometry. *Archivum Mathematicum (Brno)* **2007**, *43*, 417–429.

(17) Akbari, A.; Hill, R. J. Liquid-bridge stability and breakup on surfaces with contact-angle hysteresis. *Soft Matter* **2016**, *12*, 6868–6882.

(18) Gibbs, J. W. *Scientific Papers*; Dover: New York, 1906; Vol. 1.

(19) Butt, H.-J. private communication.

(20) Guzowski, J.; Tasinkevych, M.; Dietrich, S. Free energy of colloidal particles at the surface of sessile drops. *Eur. Phys. J. E* **2010**, *33*, 219–242.

(21) Guzowski, J.; Tasinkevych, M.; Dietrich, S. Effective interactions and equilibrium configurations of colloidal particles on a sessile droplet. *Soft Matter* **2011**, *7*, 4189–4197.

(22) Zhuang, J.; Ju, Y. S. A combined experimental and numerical modeling study of the deformation and rupture of axisymmetric liquid bridges under coaxial stretching. *Langmuir* **2015**, *31*, 10173–10182.

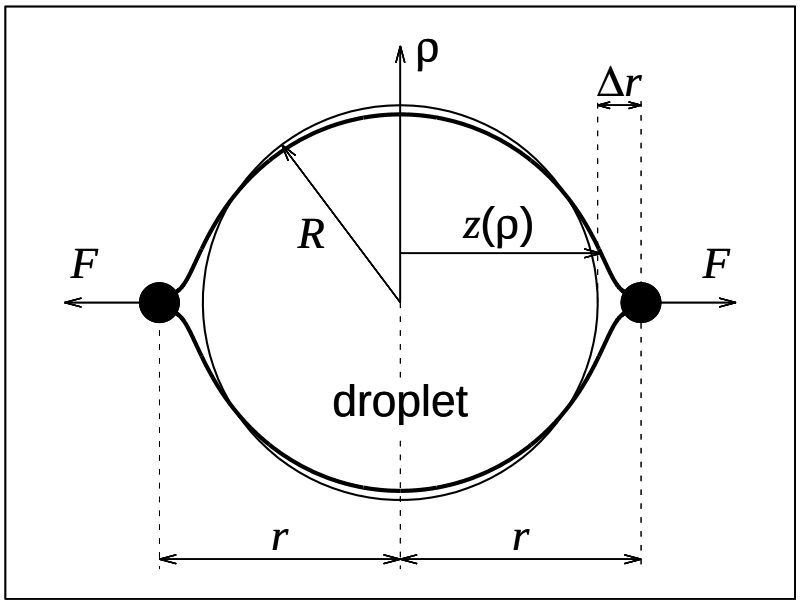

(a)

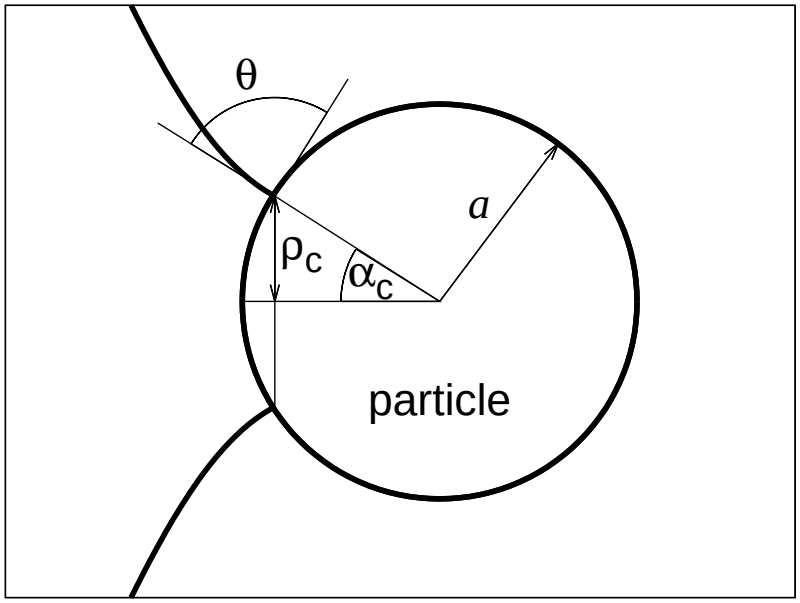

(b)

Figure 1: Geometry of the system, where the position of contact line is now fixed on the surface of particle and thus the value of angle θ alters as particles are pulled away, (a) position of particles on surface of droplet, (b) the deformation close to a particle.

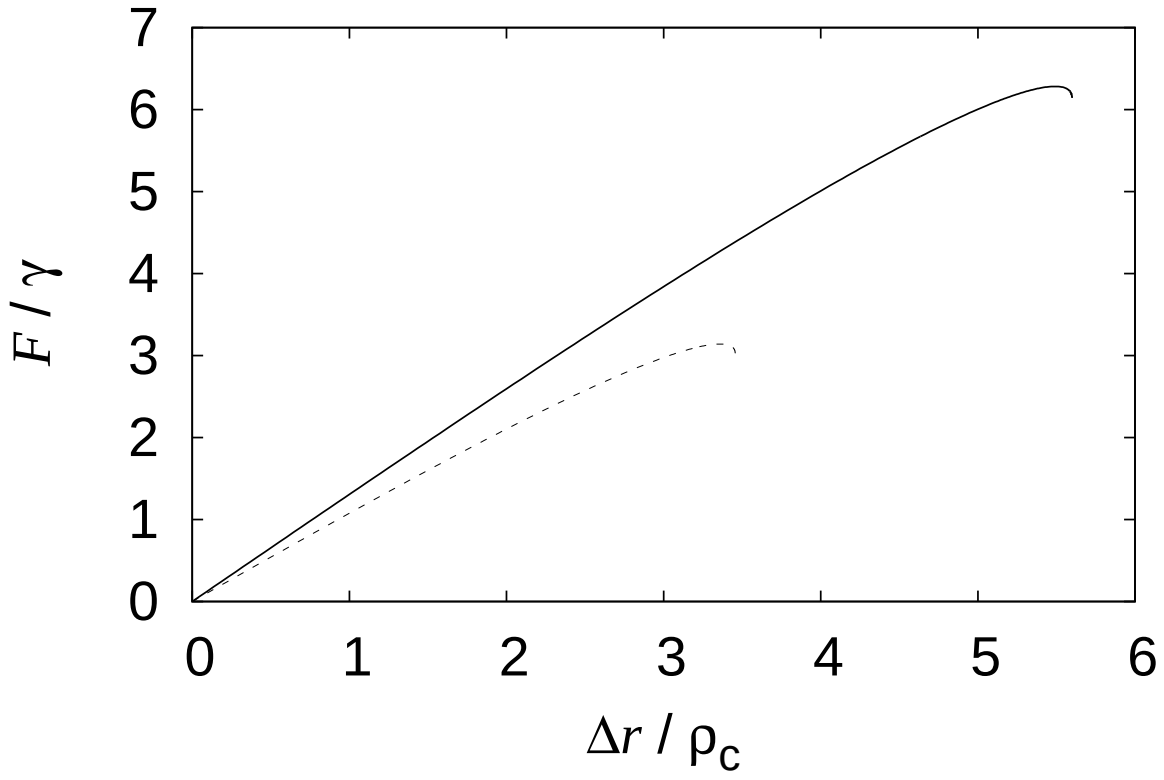

Figure 2: Displacement–force diagram for $\rho_c/R = 0.01$ (solid line). For comparison, the curve for the case of free contact line (dashed line) is shown for a 90° contact angle. The size ratio is $a/R = 0.01$, where a is the radius of the particle.

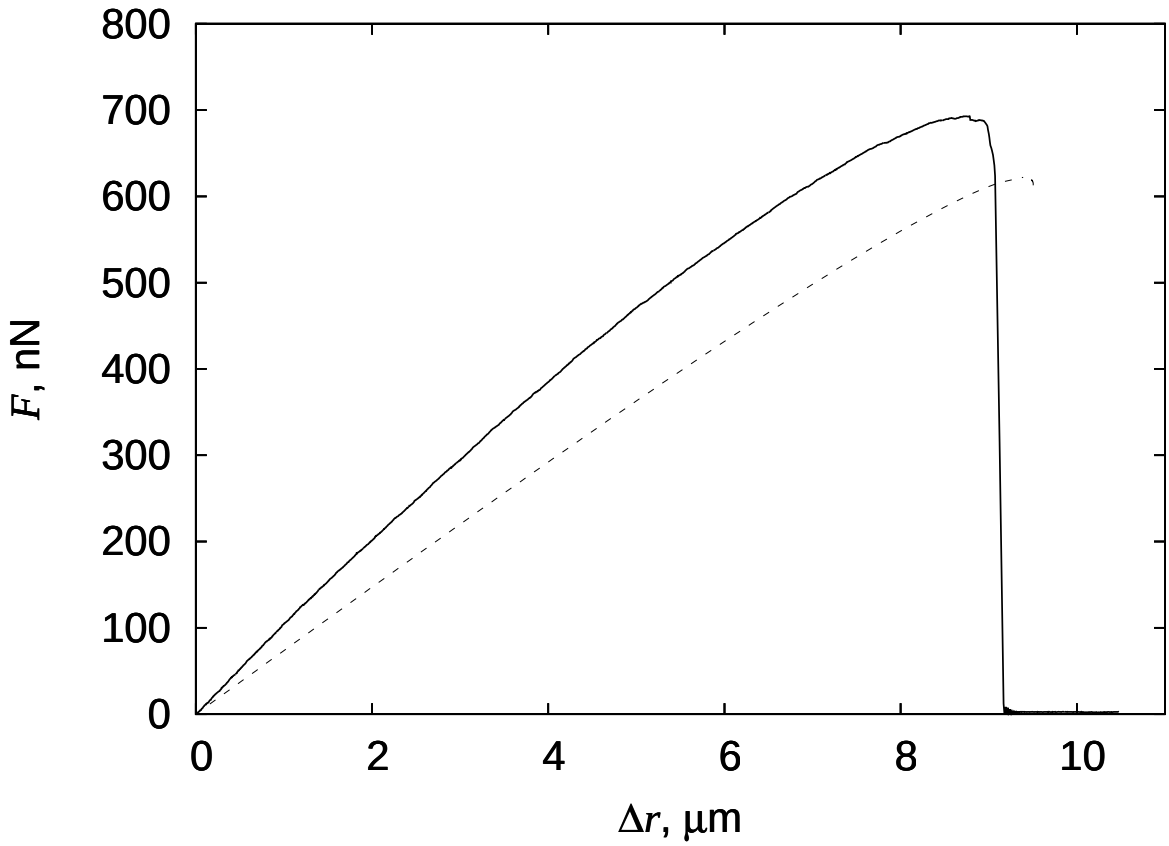

Figure 3: Experimental[10] (solid) and theoretical (dashed) displacement–force diagrams for a particle of radius $R = 1.90\,\mu$m on surface of an air bubble with volume 0.3μL. A circumferential cut is located at distance $0.31R$ from the pole of the particle. Surface tension is 0.072 N/m. The contact angle at detachment, calculated using Eq. (36), is 82°.

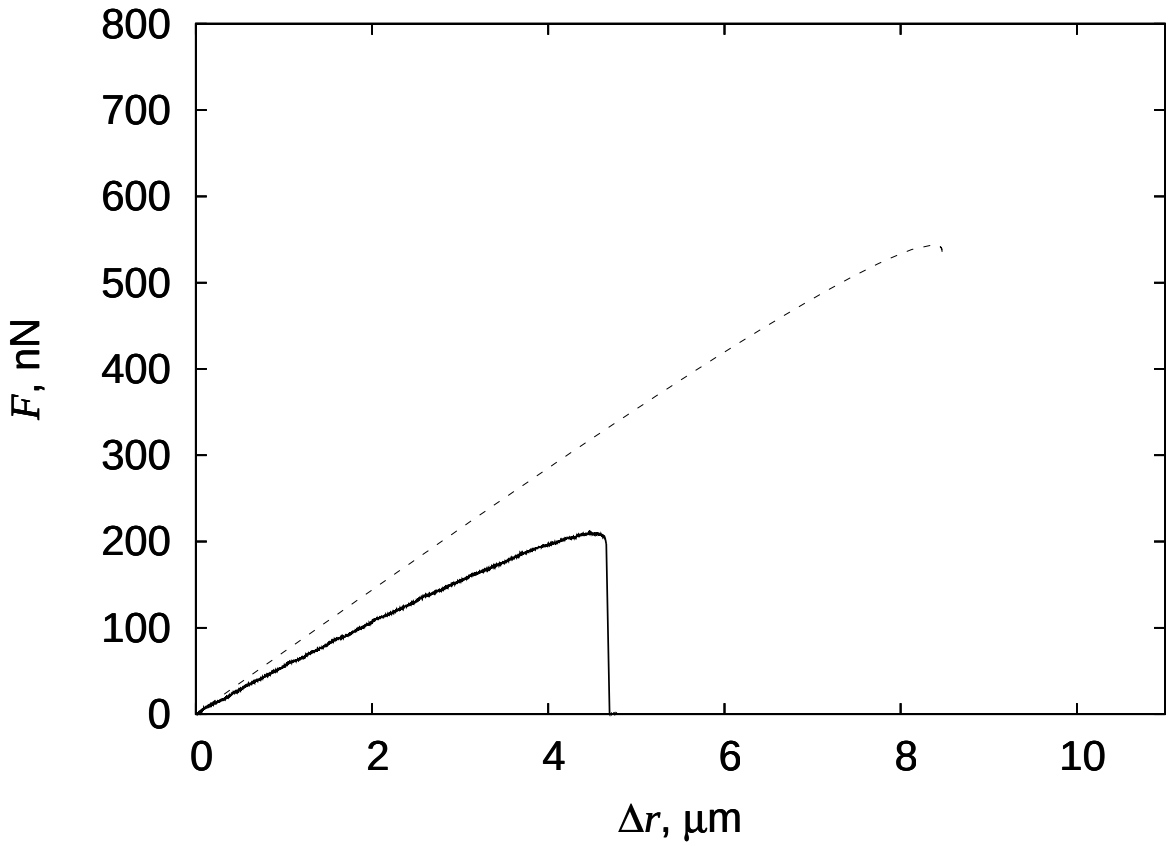

Figure 4: Experimental[10] (solid) and theoretical (dashed) displacement–force diagrams for a particle of radius $R = 1.85\,\mu$m on surface of a water droplet with volume 0.3μL. A circumferential cut is located at distance $0.24R$ from the pole of the particle. Surface tension is $0.072\,$N/m. The contact angle at detachment, calculated using Eq. (36), is 76°.

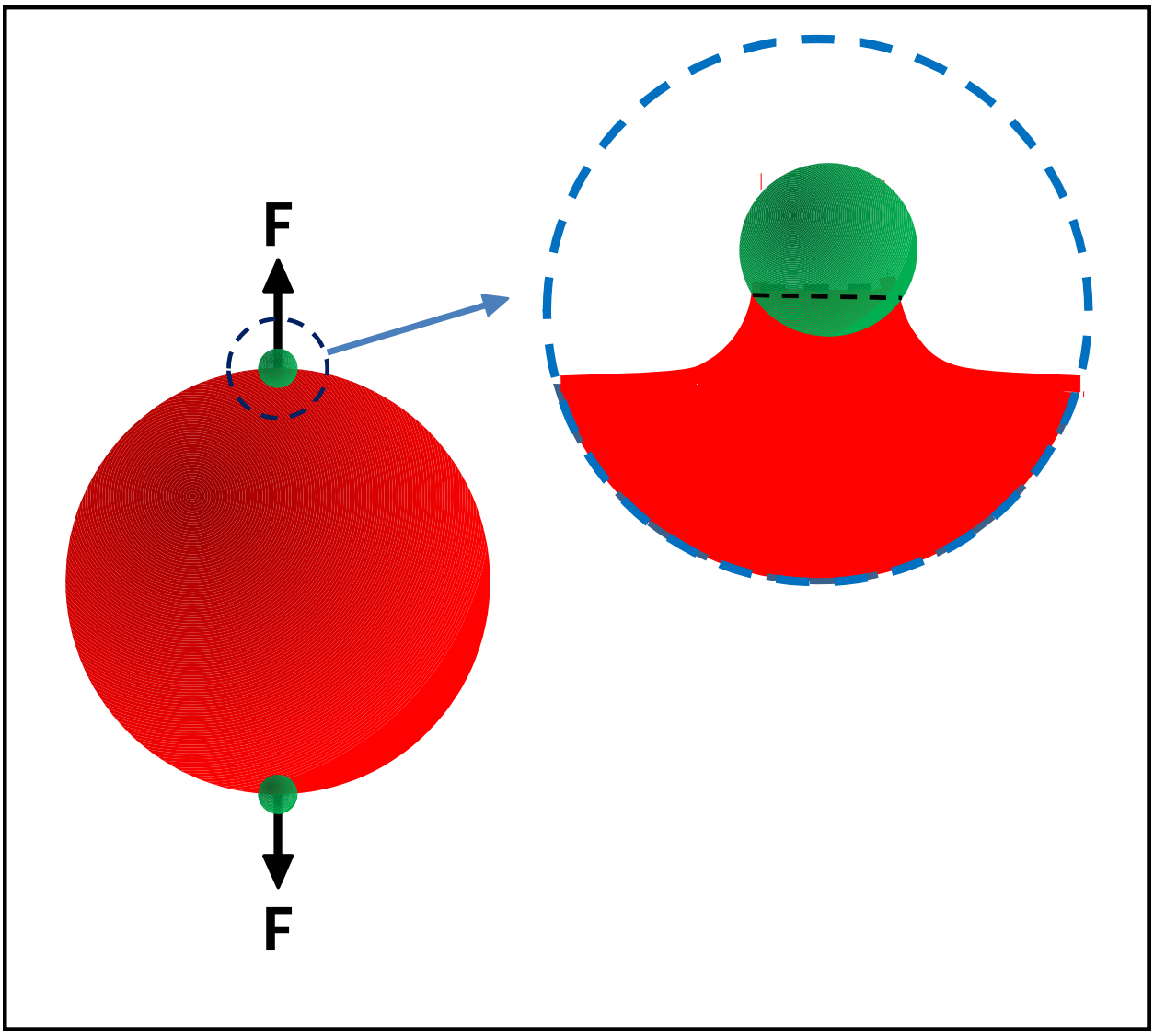

Figure 5: Graphical abstract.